Appendix A

RT2: Input parameters and file formats

A.1 Input parameters

A.1.1 Radar and surface parameters

- **Wavenumber**: $k = 2\pi/\lambda$ (ERS-1/2: λ=5.66cm $\rightarrow$ k=111.01 m^{-1}).
- **Incidence angle**: θ (ERS-1/2: $\theta = 23°$).
- **Surface roughness**: σ: root mean square vertical height of the surface.
- **Surface correlation function and correlation length**: for a 1D surface profile z(x), the surface correlation function is defined as:

$$\rho(\xi) = \frac{\int_{-L_x/2}^{L_x/2} z(x)z(x+\xi)dx}{\int_{-L_x/2}^{L_x/2} z^2(x)dx} \tag{A.1}$$

  $\rho(\xi)$ is a measure of the similarity between the height at point x=0 and the height at point x=ξ. It can be viewed as a surface 'horizontal roughness'.

  In RT2 a model surface correlation function has to be specified as one the following model function:

  - Gaussian: $\rho(\xi) = exp[-\xi^2/l^2]$
  - Exponential: $\rho(\xi) = exp[-\xi/l]$
  - 'Core-index': $\rho(\xi) = [1 + \xi^2/l^2]^{-3/2}$

  The parameter l is the surface correlation length. It is an estimate of the statistical independence of two points of the surface. For example, in the case of a perfectly smooth surface, all the points are correlated and l=∞.

- **Surface scattering model**:
  - *Small perturbation model*: applicable to slightly rough surfaces, i.e.:

  - the surface standard deviation σ is less than 5% of the wavelength: $k\sigma < 0.3$
  - the surface slope is of the same order of magnitude as $k\sigma$: $\sqrt{2}\sigma/l < 0.3$, where the term $\sqrt{2}\sigma/l$ is the rms slope assuming a Gaussian correlation function (see [18] for a full derivation).

  With the small perturbation model, an analytic expression can be derived for the backscatter coefficient, as shown in [18].

- *Kirchhoff approximation*: assumes that the reflection from a point on the surface is equivalent to the reflection from an infinite plane tangent to the local surface. It is applicable when:
  - the surface correlation length l is larger than the wavelength: $kl > 6$.
  - the surface standard deviation is small enough so the radius of curvature is larger than the wavelength: $l^2 > 2.76\sigma\lambda$ (see [18] for a derivation of this equation).

  If the Kirchhoff approximation is satisfied, two surface models can be applied, with additional conditions: the Kirchhoff geometrical optics and Kirchhoff physical optics models.

- *Kirchhoff geometrical optics*: The Kirchhoff approximation conditions must apply, as well as the additional condition: $k\sigma > 2$ (i.e. rough surface).

- *Kirchhoff physical optics*: The Kirchhoff approximation conditions must apply, as well as the additional condition: $\sqrt{2}\sigma/l < 0.25$ (i.e. medium rough surface).

  Two methods can be used in this case:
  - Physical optics 1: a Taylor expansion with respect to the surface slopes is used to estimate the surface reflection coefficients needed to calculate the backscatter coefficients.
  - Physical optics 2: the 0^{th} order approximation is used for the reflection coefficients.

- *Empirical models*: RT2 offers the possibility to use empirical models, but they cannot be used in conjunction with a vegetation layer (surface scattering only).

Figure A.1 summarises the different available models and their domain of applicability, depending on the surface correlation length l and surface standard deviation σ.

- **Susceptibility of the soil**: ε-1, where ε is the dielectric constant of the soil. The susceptibility can be supplied by the user or estimated from an empirical model presented in [70]. The inputs to the model are the volumetric moisture of the soil, and the sand/clay/silt content.

- **Air temperature**: required to calculate the vegetation permittivity.

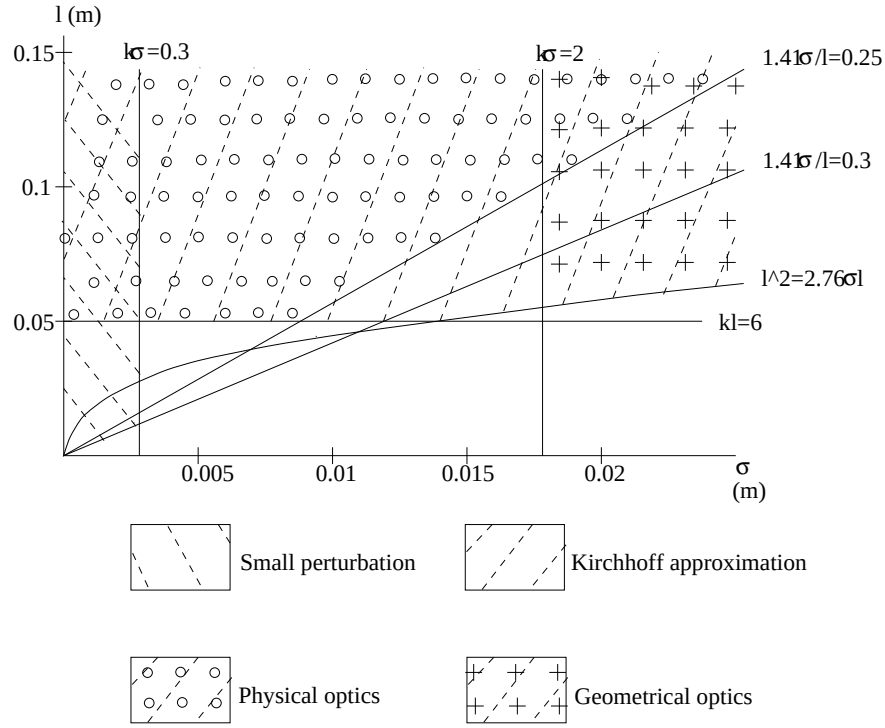

Figure A.1: Validity of the RT2 surface scattering models (plotted with the ERS value for $k \approx 111m^{-1}$)

- **Number of values**: if a parameter is varied (multi-parameter mode), this specifies the number of values to be taken by this parameter in the interval defined by a lower and upper limit.
- **Corrugated surface**: the surface can be defined to have corrugations. These are defined by their amplitude, their wavenumber, and their orientation, i.e. the orientation of the rows with respect to radar look direction.
- **Layers**: they are defined by their number (1 to 3), their depth, and their number of scatterers (1 to 5).

A.1.2 Scatterer parameters

- **Susceptibility**: As for the soil, the susceptibility of the scatterer can be supplied or modelled. In the latter case, the gravimetric moisture is required, as well as the type of model to use:
  - *'Leafy' model*: for leaf-like vegetation scatterers.
  - *'Woody' model*: for branches and trunks.
  - An earlier empirical model is also available.
- **Scatterer type**: Each scatterer type is defined by its shape, its dimensions and its number density in the layer. With the definition of the shape, the user needs to specify which approximation to use for the scattering calculations. The different approximations are:

- *Rayleigh-Gans*: $r_{min} \ll r_{max}, \lambda$
- *Rayleigh*: r_{min}, $r_{max} \ll \lambda$
- *Infinite cylinder*: $l > 10r$ ($r = r_{min} = r_{max}$)

The different available shapes are:

- *Circular disc (Rayleigh-Gans)*: $r_{min} = r_{max} = r$: radius of the disc, l: half thickness of the disc.
- *Elliptical disc (Rayleigh-Gans)*: r_{min}: semi-minor axis of the ellipse, r_{max}: semi-major axis of the ellipse, l: half thickness of the ellipse.

These first two shapes are usually used to model leaves, so $l \ll r_{min}, r_{max}$.

- *Thin needle (Rayleigh-Gans)*: same as elliptical disc with a half length of the order of r_{min} and r_{max}.
- *Infinite cylinder*: the half-length l of the cylinder is much larger then the radius of its cross-section.

These previous two shapes are used to model stems.

- *Elliptical disc (Rayleigh)*: same definition as above, here in the Rayleigh approximation.
- *Needle (Rayleigh)*: same definition as above, here in the Rayleigh approximation.
- *Disc (Rayleigh) - Ellipsoid shape*: r_{min}: semi-minor axis at the cross-section of the middle of the ellipsoid (across its principal axis), r_{max}: semi-major axis at the cross-section of the middle of the ellipsoid (across its principal axis), l: half length of the ellipsoid in the direction of the principal axis.

As for the circular and elliptical discs, the half length is smaller than the semi axes (leaf shape).

- *Needle (Rayleigh) - Ellipsoid shape*: same as the ellipsoidal disc, with the half length larger than the semi axes (stem shape).

- **Scatterer angles**: Three angles define the position of a scatterer: the inclination angle α, the axial angle δ and the orientation angle γ. They are represented on Figure A.2.

  A value of α and δ is assigned to each scatterer according to a statistical distribution to be specified by the user. The angle γ is always assumed to be uniformly distributed, i.e. there is no preferred direction for the scatterers in the horizontal plane.

  The available distributions for the inclination angle α are:

  - *Uniform*: f(α)=constant for $\mu_\alpha - 1/2r_\alpha < \alpha < \mu_\alpha + 1/2r_\alpha$ (r_α: half the total angle range, $_\alpha$: mean inclination angle)

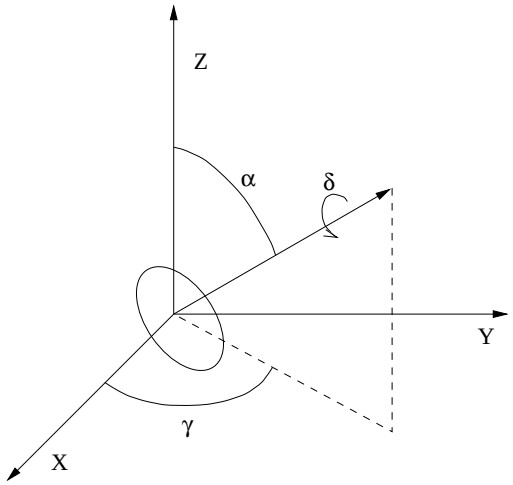

Figure A.2: Scatterers angles

- *Gaussian*: (σ_α: inclination angle standard deviation)

$$f(\alpha) = \frac{1}{\sqrt{2\pi}\sigma_\alpha} \exp\left[-\frac{1}{2}\left(\frac{\alpha - \mu_\alpha}{\sigma_\alpha}\right)^2\right] \tag{A.2}$$

- *Spherical*: $f(\alpha) = \sin(\alpha)$
- *Erectophile*: $f(\alpha) = (2/\pi)[1 + \cos(2\alpha)]$
- *Planophile*: $f(\alpha) = (2/\pi)[1 - \cos(2\alpha)]$
- *Plagiophile*: $f(\alpha) = (2/\pi)[1 - \cos(4\alpha)]$
- *Extremophile*: $f(\alpha) = (2/\pi)[1 + \cos(4\alpha)]$

The available distributions for the axial angle δ are the uniform or Gaussian distributions. The same definition as above applies, with the specification of a mean μ_δ and a spread (standard deviation σ_δ for the Gaussian distribution, and half angle range r_δ for the uniform distribution).

A.2 RT2 output file format

The outputs from the RT2 module are arranged in columns as shown in Table A.1, where P is the parameter varied (user-defined). The file contains as many lines as increments of P.

A.3 read-and-write output file format

The 'read-and-write' output file is composed of as many lines as the required number of values of the varied input parameter (similarly to the RT2 output file). It is composed of 14 columns, as shown in Table A.2, with the following nomenclature:

- 1, 2, 3: lower, middle, upper layer direct scattering.

P	Backscatter coefficients				Correlation coefficients			Penetration depths					
	HH	VV	HV	VH	HHVV amplitude	HHVV phase	HH-to-VV correlation coefficient	Layer 1		Layer 2		Layer 3	
								V	H	V	H	V	H
⋮	⋮	⋮	⋮	⋮	⋮	⋮	⋮	⋮	⋮	⋮	⋮	⋮	⋮

Table A.1: RT2 output file format

- g: direct ground scattering.
- 1g, 2g, 3g: lower layer-ground, middle layer-ground, upper layer-ground double scattering.
- 12, 13, 23: lower-middle, lower-upper, middle-upper inter layer double scattering.
- 11, 22, 33: intra-layer double scattering.

Parameter varied	1	1g	g	2	2g	12	11	22	3	3g	13	23	33
⋮	⋮	⋮	⋮	⋮	⋮	⋮	⋮	⋮	⋮	⋮	⋮	⋮	⋮

Table A.2: read-and-write output file format

A.4 RT2 summary file for the wheat simulation of Section 3.3

Number of values	10
Variable name	Incidence angle
Lower limit	10+0j
Upper limit	70+0j
Calculate susceptibility?	Yes
Related parameters?	No
Interactions	1st order/specular
1st order tolerance	1e-05
2nd order tolerance	1e-05
Rough surface tolerance	0
1st order loops	5000
2nd order loops	20
Rough surface loops	10
Tilt loop no.	5000

Upper range for integration	0.95
Lower range for integration	0
Wave number	111
Incidence angle	23
Lower layer depth	0.5
Number of layers	1
Lower layer scatterers	2
Ground model	Physical optics 1
Corrugated surface?	No
Correlation function	Gaussian
Roughness	0.006
Correlation length	0.1
Soil moisture	0.17
Sand (%)	30
Clay (%)	40
Temperature	22

Lower layer, scatterer 1

Half-length	0.25
Major axis	0.001
Minor axis	0.001
Number density	640
Mean azimuth angle	180
Spread in azimuth angle	180
Mean inclination angle	0
Spread in inclination angle	10
Mean axis orientation	0
Spread in axis orientation	90
Inclination angle distribution	Gaussian
Axial angle distribution	Uniform
Scatterer shape	Infinite cylinder
Susceptibility	0+0j
Calculate susceptibility?	Yes
Gravimetric moisture	0.72
Susceptibility model	Leafy

Lower layer, scatterer 2

Half-length	0.0001
Major axis	0.06
Minor axis	0.005
Number density	3430
Mean azimuth angle	180
Spread in azimuth angle	180
Mean inclination angle	45
Spread in inclination angle	45
Mean axis orientation	0

Spread in axis orientation	90
Inclination angle distribution	Uniform
Axial angle distribution	Uniform
Scatterer shape	Elliptical disc (Rayleigh-Gans)
Susceptibility	0+0j
Calculate susceptibility?	Yes
Gravimetric moisture	0.67
Susceptibility model	Leafy

Appendix B

Singular Value Decomposition of a matrix and application to the solution of linear equations

Singular Value Decomposition (SVD) methods are based on the following theorem: any MxN matrix $\mathbf{A}$ can be written as the product of an MxN column orthogonal matrix $\mathbf{U}$, an NxN diagonal matrix with positive (or null) elements which are the singular values of $\mathbf{A}$, and the transpose of an NxN orthogonal matrix $\mathbf{V}$:

$$\mathbf{A} = \mathbf{U}.\mathbf{W}.\mathbf{V}^T \tag{B.1}$$

It is beyond the scope of this section to prove the theorem or to make a comprehensive presentation of the properties associated with the matrices of Equation (B.1) and with the singular values w_k.

First, in the case of an NxN *square* matrix $\mathbf{A}$, SVD can be used to solve linear equations of the type $\mathbf{A}.\mathbf{x} = \mathbf{b}$, where $\mathbf{x}$ and $\mathbf{b}$ are N-vectors. The matrix $\mathbf{A}$ is a linear mapping of the vector space $\mathbf{x}$ to the vector space $\mathbf{b}$. If one or more of the singular values of $\mathbf{A}$ is equal to 0 (w_k=0 for some k$\in \{1, \ldots, N\}$), then $\mathbf{A}$ is singular and there is a subspace of $\mathbf{x}$ such that $\mathbf{A}.\mathbf{x} = \mathbf{0}$. The number of singular values of $\mathbf{A}$ gives the dimension of that subspace, called the nullspace. If there are s null singular values in $\mathbf{A}$, then there is a subspace of $\mathbf{x}$ of dimension N-s which maps to a subspace of $\mathbf{b}$ of the same dimension N-s. This subspace of $\mathbf{b}$ is called the range of $\mathbf{A}$ and its dimension N-s is the rank of $\mathbf{A}$. The matrices $\mathbf{U}$ and $\mathbf{V}$ can be easily used to construct orthonormal bases for the nullspace and the range of $\mathbf{A}$.

Any column of $\mathbf{V}$ whose number j is such that w_j=0 is a solution to the equation $\mathbf{A}.\mathbf{x} = \mathbf{0}$. To solve the equation $\mathbf{A}.\mathbf{x} = \mathbf{b}$ with $\mathbf{b} \neq \mathbf{0}$, two cases must be considered. If $\mathbf{b}$ is in the range of $\mathbf{A}$, then there is an exact solution to the equation. It can also be shown that there is actually a whole set of solutions since any linear combination of vectors in the nullspace can be added to a solution of $\mathbf{A}.\mathbf{x} = \mathbf{b}$ to form another solution. The solution of smallest Euclidian norm $\| \mathbf{x} \|$ is found by inverting (B.1) and replacing $1/w_j$ by 0 in $\mathbf{W}^{-1}$ when w_j=0:

$$\mathbf{x} = \mathbf{V}.\mathbf{W}^{-1}.\mathbf{U}^T.\mathbf{b} \tag{B.2}$$

with

$$\begin{array}{rcll} \mathbf{W}^{-1} & = & diag(1/w_j) & if w_j \neq 0 \\ & = & 0 & if w_j = 0 \end{array} \tag{B.3}$$

If $\mathbf{b}$ is not in the range of $\mathbf{A}$, then there is no solution to $\mathbf{A}.\mathbf{x} = \mathbf{b}$. But there is a vector $\mathbf{x}$ such that the residual $r = \| \mathbf{A}.\mathbf{x} - \mathbf{b} \|$ is minimum. This value of $\mathbf{x}$ also corresponds to the solution of Equations (B.2) and (B.3).

All proofs of the properties presented here can be found in [56]. They were presented in the case of square matrix but they also apply for rectangular matrices. In the case of Equation (4.23), there are more equations than unknowns. This case is equivalent to the case of a square matrix based on the rectangular matrices $\mathbf{A}$ or $\mathbf{E}$ and completed by columns of zeros to make it square. Then the squared matrices $\mathbf{A_s}$ and $\mathbf{E_s}$ have as many singular values as columns of zeros, and we fall in the case where the vectors $\mathbf{b}$ and $\mathbf{c}$ are not in the range of $\mathbf{A_s}$ and $\mathbf{E_s}$ respectively but the "solutions" given by (B.2) and (B.3) are effectively least-square solutions as they minimises the Euclidian norms $\| \mathbf{A}.\mathbf{p_0} - \mathbf{b} \|$ and $\| \mathbf{E}.\mathbf{p}' - \mathbf{c} \|$.

In practice, i.e. for numerical solving, some singular values may not be exactly equal to 0 but very small. These values must be set to 0 manually before the backsubstitution (Equation (B.2)) can be performed. The threshold defining "small" for a singular value depends on the application.

Appendix C

Correlation coefficient in the 3D colour space

The definition of the correlation coefficient between two sets of pixels defined by their red, green and blue bands originates from the standard definition of the correlation coefficient r in the one-dimensional case. In the case of two series of N data points x_i and y_i, r is defined in [68] as:

$$r = \frac{S_{xy}}{\sqrt{S_{xx} S_{yy}}} \tag{C.1}$$

with:

$$\begin{aligned} S_{xx} &= \sum_{i=1}^{N} x_i^2 - \frac{\left(\sum_{i=1}^{N} x_i\right)^2}{N} \\ S_{yy} &= \sum_{i=1}^{N} y_i^2 - \frac{\left(\sum_{i=1}^{N} y_i\right)^2}{N} \\ S_{xy} &= \sum_{i=1}^{N} x_i y_i - \frac{\left(\sum_{i=1}^{N} x_i\right)\left(\sum_{i=1}^{N} y_i\right)}{N} \end{aligned} \tag{C.2}$$

In the case dealt with here the scalar values x_i and y_i are replaced by vectors defining the three colour bands of a pixel. $\mathbf{x}_i(b_{x_i}, g_{x_i}, r_{x_i})$ and $\mathbf{y}_i(b_{y_i}, g_{y_i}, r_{y_i})$ are used, where b, g and r and the values in blue, green, and red bands respectively. The same definition for the correlation coefficient holds (Equation C.1), with the following definition for S_{xx}, S_{yy}, and S_{xy}:

$$S_{xx} = \sum_{i=1}^{N} \mathbf{x}_i^2 - \frac{\left(\sum_{i=1}^{N} \mathbf{x}_i\right)^2}{N}$$

$$= \sum_{i=1}^{N}\left(b_{x_i}^2 + g_{x_i}^2 + r_{x_i}^2\right) - \frac{1}{N}\left[\left(\sum_{i=1}^{N} b_{x_i}\right)^2 + \left(\sum_{i=1}^{N} g_{x_i}\right)^2 + \left(\sum_{i=1}^{N} r_{x_i}\right)^2\right] \quad \text{(C.3)}$$

$$S_{yy} = \sum_{i=1}^{N}\mathbf{y}_i^2 - \frac{\left(\sum_{i=1}^{N}\mathbf{y}_i\right)^2}{N}$$

$$= \sum_{i=1}^{N}\left(b_{y_i}^2 + g_{y_i}^2 + r_{y_i}^2\right) - \frac{1}{N}\left[\left(\sum_{i=1}^{N} b_{y_i}\right)^2 + \left(\sum_{i=1}^{N} g_{y_i}\right)^2 + \left(\sum_{i=1}^{N} r_{y_i}\right)^2\right] \quad \text{(C.4)}$$

$$S_{xy} = \sum_{i=1}^{N}\mathbf{x}_i\mathbf{y}_i - \frac{\left(\sum_{i=1}^{N}\mathbf{x}_i\right)\left(\sum_{i=1}^{N}\mathbf{y}_i\right)}{N}$$

$$= \sum_{i=1}^{N}\left(b_{x_i}b_{y_i} + g_{x_i}g_{y_i} + r_{x_i}r_{y_i}\right)$$

$$-\frac{1}{N}\left[\left(\sum_{i=1}^{N} b_{x_i}\right)\left(\sum_{i=1}^{N} b_{y_i}\right) + \left(\sum_{i=1}^{N} g_{x_i}\right)\left(\sum_{i=1}^{N} g_{y_i}\right)\right.$$

$$\left. + \left(\sum_{i=1}^{N} r_{x_i}\right)\left(\sum_{i=1}^{N} r_{y_i}\right)\right] \quad \text{(C.5)}$$

Appendix D

Clock board connections and layout

Nomenclature :

- '390: frequency divider 74HC390N
- '393: frequency divider 74HC393N
- '151: multiplexer 74HC151N
- '04: Schmitt triggers 74HC04N

The switch truth table is:

Switch position	Switch bit values			Selected multiplexer channel	Selected frequency (Hz)
	1	2	3		
1	1	0	0	G	100
2	0	1	0	F	40
3	1	1	0	E	20
4	0	0	1	D	10
5	1	0	1	C	5
6	0	1	1	B	2
7	1	1	1	A	1

Table D.1: Relation between the switch position and the selected channel of the multiplexer

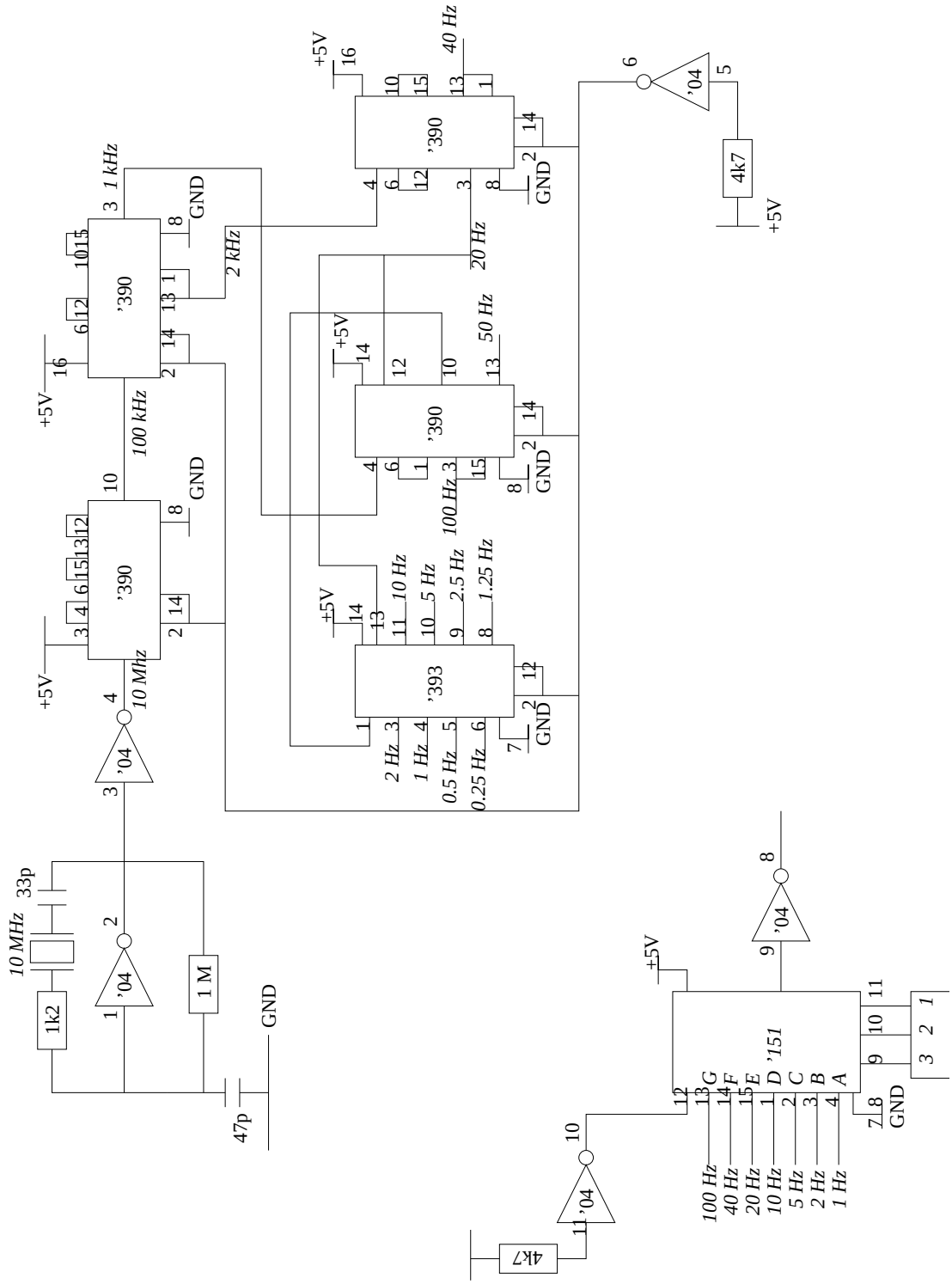

Figure D.1: Connections on the clock board

Appendix E

Conversion from the DVA wind speed readings into a wind velocity vector

Let $(\mathbf{e_x}, \mathbf{e_y}, \mathbf{e_z})$ be the unit vectors defining the (X,Y,Z) coordinate system, and $(\mathbf{e_1}, \mathbf{e_2}, \mathbf{e_3})$ be the unit vectors normal to the DVA $n°1$, 2 and 3 respectively (see Figure 5.2). According to Table 5.1:

$$\begin{pmatrix} e_1 \\ e_2 \\ e_3 \end{pmatrix} = \begin{pmatrix} \sqrt{\frac{2}{3}} & \frac{1}{2} & -\frac{1}{2\sqrt{3}} \\ \sqrt{\frac{2}{3}} & -\frac{1}{2} & -\frac{1}{2\sqrt{3}} \\ \sqrt{\frac{2}{3}} & 0 & \frac{1}{\sqrt{3}} \end{pmatrix} . \begin{pmatrix} e_x \\ e_y \\ e_z \end{pmatrix} = \begin{pmatrix} a_{11} & a_{12} & a_{13} \\ a_{21} & a_{22} & a_{23} \\ a_{31} & a_{32} & a_{33} \end{pmatrix} . \begin{pmatrix} e_x \\ e_y \\ e_z \end{pmatrix} = \mathbf{A}. \begin{pmatrix} e_x \\ e_y \\ e_z \end{pmatrix} \tag{E.1}$$

The total wind velocity $\mathbf{w}$ has three components in the (X,Y,Z) coordinate system:

$$\mathbf{w} = w_x.\mathbf{e_x} + w_y.\mathbf{e_y} + w_z.\mathbf{e_z} \tag{E.2}$$

and the wind readings w_1, w_2, w_3 from the three DVAs of a triad define the wind vectors $\mathbf{w_1}$, $\mathbf{w_2}$, and $\mathbf{w_3}$, such that:

$$\begin{aligned} \mathbf{w_1} &= w_1.\mathbf{e_1} \\ \mathbf{w_2} &= w_2.\mathbf{e_2} \\ \mathbf{w_3} &= w_3.\mathbf{e_3} \end{aligned} \tag{E.3}$$

Let the matrix $\mathbf{B}$ be the inverse of $\mathbf{A}$:

$$\mathbf{B} = \mathbf{A}^{-1} = \begin{pmatrix} b_{11} & b_{12} & b_{13} \\ b_{21} & b_{22} & b_{23} \\ b_{31} & b_{32} & b_{33} \end{pmatrix} \tag{E.4}$$

Therefore:

$$\begin{pmatrix} e_x \\ e_y \\ e_z \end{pmatrix} = \mathbf{B}. \begin{pmatrix} e_1 \\ e_2 \\ e_3 \end{pmatrix} \tag{E.5}$$

Hence, from Equation (E.2),

$$\begin{aligned} \mathbf{w} = \quad & w_x b_{11}.\mathbf{e_1} + w_x b_{12}.\mathbf{e_2} + w_x b_{13}.\mathbf{e_3} \\ & + w_y b_{21}.\mathbf{e_1} + w_y b_{22}.\mathbf{e_2} + w_y b_{23}.\mathbf{e_3} \\ & + w_z b_{31}.\mathbf{e_1} + w_z b_{32}.\mathbf{e_2} + w_z b_{33}.\mathbf{e_3} \end{aligned} \tag{E.6}$$

The measured wind vectors $\mathbf{w_i}$ are the projection of the total wind vector $\mathbf{w}$ on the normal axes of the DVAs $\mathbf{e_i}$. This translates into the following relations:

$$\begin{aligned} w_1 = \mathbf{w}.\mathbf{e_1} = \; & w_x b_{11} + w_y b_{21} + w_z b_{31} \\ & + (w_x b_{12} + w_y b_{22} + w_z b_{32})\,(\mathbf{e_2}.\mathbf{e_1}) \\ & + (w_x b_{13} + w_y b_{23} + w_z b_{33})\,(\mathbf{e_3}.\mathbf{e_1}) \end{aligned} \tag{E.7}$$

$$\begin{aligned} w_2 = \mathbf{w}.\mathbf{e_2} = \; & w_x b_{12} + w_y b_{22} + w_z b_{32} \\ & + (w_x b_{11} + w_y b_{21} + w_z b_{31})\,(\mathbf{e_1}.\mathbf{e_2}) \\ & + (w_x b_{13} + w_y b_{23} + w_z b_{33})\,(\mathbf{e_3}.\mathbf{e_2}) \end{aligned} \tag{E.8}$$

$$\begin{aligned} w_3 = \mathbf{w}.\mathbf{e_3} = \; & w_x b_{13} + w_y b_{23} + w_z b_{33} \\ & + (w_x b_{11} + w_y b_{21} + w_z b_{31})\,(\mathbf{e_1}.\mathbf{e_3}) \\ & + (w_x b_{12} + w_y b_{22} + w_z b_{32})\,(\mathbf{e_2}.\mathbf{e_3}) \end{aligned} \tag{E.9}$$

With, from Equation (E.1):

$$\begin{aligned} \mathbf{e_1}.\mathbf{e_2} &= a_{11}a_{21} + a_{12}a_{22} + a_{13}a_{23} \\ \mathbf{e_1}.\mathbf{e_3} &= a_{11}a_{31} + a_{12}a_{32} + a_{13}a_{33} \\ \mathbf{e_2}.\mathbf{e_3} &= a_{21}a_{31} + a_{22}a_{32} + a_{23}a_{33} \end{aligned} \tag{E.10}$$

Equations (E.7) to (E.9) can be written in a more compact matrix form:

$$\begin{pmatrix} w_1 \\ w_2 \\ w_3 \end{pmatrix} = \left[\mathbf{B}^T + (\mathbf{e_1}.\mathbf{e_2})\,.\mathbf{C_{12}} + (\mathbf{e_1}.\mathbf{e_3})\,.\mathbf{C_{13}} + (\mathbf{e_2}.\mathbf{e_3})\,.\mathbf{C_{23}}\right] . \begin{pmatrix} w_x \\ w_y \\ w_z \end{pmatrix} = \mathbf{D}. \begin{pmatrix} w_x \\ w_y \\ w_z \end{pmatrix} \tag{E.11}$$

where $\mathbf{B^T}$ is the transpose of $\mathbf{B}$ and $\mathbf{C_{12}}$, $\mathbf{C_{13}}$, $\mathbf{C_{23}}$ are defined as follows:

$$\mathbf{C_{12}} = \begin{pmatrix} b_{12} & b_{22} & b_{32} \\ b_{11} & b_{21} & b_{31} \\ 0 & 0 & 0 \end{pmatrix} \tag{E.12}$$

$$\mathbf{C_{13}} = \begin{pmatrix} b_{13} & b_{23} & b_{33} \\ 0 & 0 & 0 \\ b_{11} & b_{21} & b_{31} \end{pmatrix} \tag{E.13}$$

and

$$\mathbf{C_{23}} = \begin{pmatrix} 0 & 0 & 0 \\ b_{13} & b_{23} & b_{33} \\ b_{12} & b_{22} & b_{32} \end{pmatrix} \tag{E.14}$$

The wind velocity coordinates in the (X,Y,Z) reference are obtained by inverting the matrix $\mathbf{D}$:

$$\begin{pmatrix} w_x \\ w_y \\ w_z \end{pmatrix} = \mathbf{D^{-1}}. \begin{pmatrix} w_1 \\ w_2 \\ w_3 \end{pmatrix} \tag{E.15}$$

Appendix F

Wind and video data storage

F.1 Camera parameters

The camera positions and orientation angles for the different recording dates are given in Tables F.1 and F.2. The coordinates of camera i ($i = 1, 2$) in the fixed reference system are x_i, y_i, z_i, expressed in cm. The inclination, azimuth, and tilt angles are θ_i, ϕ_i and ψ_i respectively. They are defined in Figure 4.1, and expressed in radians. Table F.3 gives the distance between the two cameras in cm, directly measured during the field experiments with an estimated accuracy of about $\pm$ 1 cm.

Date	x_1 (cm)	y_1 (cm)	z_1 (cm)	θ_1 (rad)	ϕ_1 (rad)	ψ_1 (rad)
1^{st} May	-65.0	-48.9	-27.2	0.66	0.13	0.00
6^{th} June	-62.8	-87.6	69.0	0.94	-0.46	0.0
21^{st} June	-6.9	107.0	59.4	-1.45	-0.50	-0.03
19^{th} July	16.9	-91.2	68.5	1.98	-0.54	0.00
25^{th} July	-19.6	-110.9	50.2	1.52	-0.43	0.00
2^{nd} August	-38.8	-80.3	59.6	1.14	-0.55	0.08
15^{th} August	-62.2	-81.0	60.6	0.88	-0.57	0.06

Table F.1: Camera 1 coordinates and orientation angles determined for recording dates

F.2 Wind data parameters

Table F.4 gives the distance between the DVA triads, when several of them were in use, and the height of the triads above the ground for each recording dates. The distances between triads is defined according to Figure 6.1. d_{ij} is the distance between triad i and j and h_t is the height of triad t, measured between the surface and the triad mount. Note that on 21^{st} June, the triads 1T and 3 were mounted on the same pole, so their relative distance is 0. Table F.5 gives the line number L in the wind data files corresponding in time to the first line of the target position files. The value of L is the result of the time synchronisation of the two data sets with

Date	x_2 (cm)	y_2 (cm)	z_2 (cm)	θ_2 (rad)	ϕ_2 (rad)	ψ_2 (rad)
1^{st} May	-12.0	-63.0	1.62	1.29	-0.19	-0.35
6^{th} June	-101.6	-38.2	68.3	0.40	-0.50	0.07
21^{st} June	-118.0	60.8	65.1	-0.60	-0.47	-0.07
19^{th} July	78.9	-37.9	66.4	2.63	-0.50	-0.03
25^{th} July	-96.7	-92.0	46.4	0.88	-0.37	-0.00
2^{nd} August	40.9	-91.5	54.7	1.83	-0.53	0.04
15^{th} August	-97.5	-18.2	58.6	0.19	-0.54	-0.04

Table F.2: Camera 2 coordinates and orientation angles determined for recording dates

Date	$d_{C_1C_2}$ (cm)
1^{st} May	62
6^{th} June	73
21^{st} June	123
19^{th} July	81
25^{th} July	80
2^{nd} August	81
15^{th} August	75

Table F.3: Distance between the two cameras measured during the field measurements

the LED, described in section 6.1.1. The values $t_{LED/on}$ and $t_{LED/off}$ also in Table F.5 give the times at which off/on and on/off transitions of the LED are seen in the video tape. The time origin of these values corresponds to the first line of the wind data files. So from $t_{LED/on}$ and $t_{LED/off}$, it is possible to synchronise the wind and video data sets, in the same way used for the one-minute sequences processed for the research.

F.3 Data files

The data files are available from the attached CD. They are in the directory 'Data'. It is structured as follows, where the names in italic are the data files and the names in normal font are the directories:

Data → 1^{st} May
6^{th} June
21^{st} June
19^{th} July → *wind velocity coordinates.txt*
25^{th} July *target1_coordinates.txt*
2^{nd} August *target2_coordinates.txt*
15^{th} August etc...

Date	Available triads	d_{12}	d_{13}	d_{23}	h_{1T}	h_{1B}	h_2	h_3
		(cm)						
6^{th} June	1T, 1B, 2, 3	110	95	113	140	80	78	76
21^{st} June	1T, 3		0		162			94
19^{th} July	3							91
25^{th} July	3							90
2^{nd} August	3							90
15^{th} August	3							87

Table F.4: Distances between DVA triads and triad height

Date	L	$t_{LED/on}$	$t_{LED/off}$
6^{th} June	970	1mn34s	1mn32s
21^{st} June	1600	1mn36s	1mn34s
19^{th} July	500	0mn36s	0mn38s
25^{th} July	1100	0mn40s	0mn42s
2^{nd} August	1180	0mn56s	0mn58s
15^{th} August	900	0mn28s	0mn30s

Table F.5: Wind data line corresponding to the first line of the target position data and time of the LED on/off transition visible in the on the video tapes (t=0 corresponds to the first line of the wind data file)

The data are stored in standard text files. The wind data files are structured in columns giving the data line number, and the coordinates w_tx, w_ty, w_tz of the measured wind velocity vector from the triad t in $m.s^{-1}$. For example, the beginning of the wind data file from August 2^{nd} is:

Data line	w3x	w3y	w3z
0	3.04827	1.33650	-0.350740
1	2.60185	0.972000	-0.561184
2	2.20503	0.607500	-0.631332
⋮	⋮	⋮	⋮

The sampling rate of the wind data is 5 Hz.

The target coordinate files have 4 columns, giving the frame number and the coordinates of the vector $\mathbf{p}'$, which is the position of the target relative to a point P_0 in the measurement volume (see section 4.2 for details). The first line of the file contains the coordinates of this point P_0, for the frame number '-1'. Coordinates are given in cm. For example, the beginning of the target 2 coordinate file from August 2^{nd} is:

Frame	x	y	z
-1	-6.35938	6.61071	-2.41264
0	-0.288998	-0.733108	0.323831
1	-0.496256	-0.889907	0.109295
2	-0.682794	-1.23616	0.0846297
⋮	⋮	⋮	⋮

Appendix G

Calculation of the wheat static deflection

G.1 Theoretical modelling

This section gives an analytic expression of the wheat deflection subject to a constant wind force. After an introduction to the variables, the wheat shape function is presented.

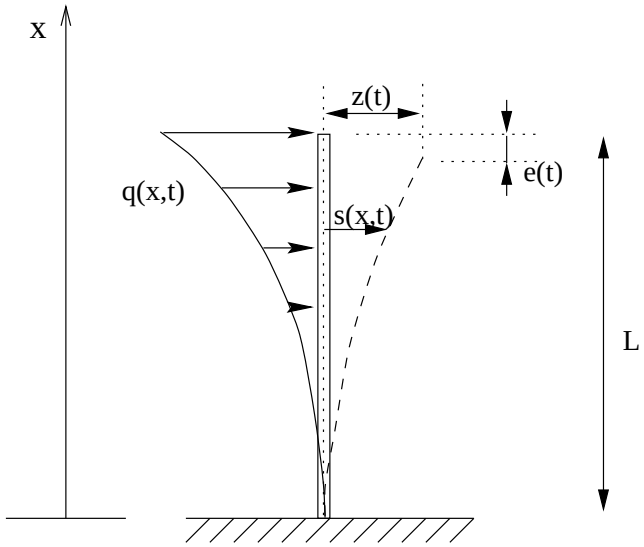

Figure G.1: Vertical beam subject to external wind loading

The approach used here considers a wheat plant as a vertical beam (in its initial position) of total length L, subject to a distributed force representing the wind loading. The beam is fixed at one of its end and free at the other end. Figure G.1 shows the model and the associated axes. The vertical axis is called x, and the deflection of the beam at height x is denoted $\psi(x)$. The distribution of the wind-induced force is denoted $q(x)$ $(N.m^{-1})$. It will be shown later that the distributed force takes the form:

$$q(x) = \frac{q_0}{L^2}x^2 \tag{G.1}$$

The beam has a mass per unit length $m(x)$ $(kg.m^{-1})$ and a flexural stiffness $EI(x)$, where E is the modulus of elasticity of the beam material and I(x) is the area moment of inertia at coordinate x. Since the wheat stalk and the wheat head have different properties in terms of mass and flexural rigidity, 2 shape functions ψ_s and ψ_h will be determined for the stalk and the head respectively. For that reason, the subscripts s and h are introduced here to refer to these two elements of the plant.

Shape function of the wheat stalk

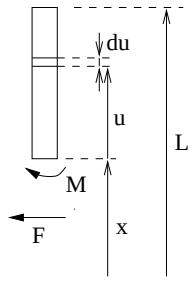

Figure G.2: Free body diagram for the wheat stalk

From the free-body diagram of Figure G.2, the moment at coordinate x along the stalk can be written:

$$M_s(x) = -\int_0^{L_s-x} q_s(u)udu = -\frac{q_{0s}}{L_s^2}\int_0^{L_s-x} u^3du = -\frac{q_{0s}}{4L_s^2}(L_s-x)^4 \tag{G.2}$$

In the case of static loads, the second derivative of the shape function $\psi_s(x)$ is related to the moment by [71]:

$$\psi_s''(x) = -\frac{M_s}{E_sI_s} \tag{G.3}$$

So in the case described here, Equation (G.3) becomes:

$$\psi_s''(x) = \frac{q_{0s}}{4E_sI_sL_s^2}(L_s-x)^4 \tag{G.4}$$

Integration of Equation (G.4) gives:

$$\psi_s'(x) = -\frac{q_{0s}}{20E_sI_sL_s^2}(L_s-x)^5 + A \tag{G.5}$$

where A is a constant. The stalk being assumed to be vertical at its base, the condition $\psi_s'(0) = 0$ is met, so $A = (q_{0s}/20E_sI_s)L_s^3$. Hence:

$$\psi_s'(x) = -\frac{q_{0s}}{20E_sI_sL_s^2}\left[(L_s-x)^5 - L_s^5\right] \tag{G.6}$$

The same process is repeated to derive $\psi_s(x)$, with the boundary condition $\psi_s(0) = 0$, giving the following expression for the shape function of the wheat stalk:

$$\psi_s(x) = \frac{q_{0s}}{120E_sI_sL_s^2}\left[(L_s-x)^6 + 6L_s^5x - L_s^6\right] \tag{G.7}$$

Shape function of the wheat head

An identical approach than for the stalk is used here. However the wind load function takes a different expression to account for the fact the base of the wheat head is shifted by a distance L_s from the origin of the x axis:

$$q_h(x) = \frac{q_{0h}}{L_h^2}(x - L_s)^2 + q_{0s} \tag{G.8}$$

The bending moment in the wheat head is defined in a similar way as in Equation (G.2), and $\psi_h''(x)$ is also derived from Equation (G.3):

$$\psi_h''(x) = \frac{q_{0h}}{12E_hI_hL_h^2}(L_h - x)^3(4L - L_h - 3x) - \frac{q_{0s}}{2E_hI_h}(L - x)^2 \tag{G.9}$$

The boundary conditions necessary in the integration are $\psi_h'(L_s) = \psi_s'(L_s)$ (continuity in the variation of the shape) and $\psi_h(L_s) = \psi_s(L_s)$ (the head being attached to the stalk). From these conditions the integration yields:

$$\psi_h'(x) = -\frac{q_{0h}}{60E_hI_hL_h^2}(L_h - x)^4(5L - 2L_h - 3x) + \frac{q_{0s}}{6E_hI_h}(L - x)^3 + A \tag{G.10}$$

and

$$\psi_h(x) = \frac{q_{0h}}{120E_hI_hL_h^2}(L_h - x)^5(2L - L_h - x) - \frac{q_{0s}}{24E_hI_h}(L - x)^4 + Ax + B \tag{G.11}$$

with:

$$\begin{aligned} A &= \frac{q_{0s}}{2}\left(\frac{L_s^3}{10E_sI_s} - \frac{L_h^3}{3E_hI_h}\right) + \frac{q_{0h}}{60E_hI_hL_h^2}(L_h - L_s)^4(3L_h + 2L_s) \\ B &= \frac{q_{0s}}{24}\left(\frac{L_s^4}{E_sI_s} + \frac{L_h^4}{E_hI_h}\right) - \frac{q_{0h}}{120E_hI_hL_h^2}(L_h - L_s)^5(L_s + L_h) - AL_s \end{aligned} \tag{G.12}$$

G.2 Numerical application for a mature wheat plant

Geometry of the wheat plant

The geometry of the wheat plant is defined by the stalk and head lengths L_s and L_h, and by their radius R_s and R_h. These values represent the cylinders of constant radius which are assumed for the shape of the stalk and the head. The values chosen for a full growth stage were measured on a typical wheat plant:

$$\begin{aligned} L_s &= 0.7 \quad m \\ L_h &= 0.07 \quad m \\ R_s &= 0.003 \quad m \\ R_h &= 0.007 \quad m \end{aligned}$$

Mass and flexural rigidity

The total masses M_s and M_h of the stalk and the head at full growth stage are taken to be 0.05 kg and 0.05 kg respectively. The mass distribution of the cylinders is assumed to be constant along their principal axis, so the masses per unit length m_s and m_h are also constant:

$$\begin{aligned} m_s &= \frac{M_s}{L_s} \quad kg.m^{-1} \\ m_h &= \frac{M_h}{L_h} \quad kg.m^{-1} \end{aligned}$$

The area moment of area for a disc is well defined in most textbooks dealing with structural analysis [71]:

$$I_s = \frac{\pi R_s^4}{4}$$

$$I_s = \frac{\pi R_s^4}{4}$$

The modulus of elasticity for the stalk and the head, E_s and E_h, is more challenging to estimate since, to the knowledge of the author, it has not been documented. Consequently, estimates must be made. For that purpose it is useful to quote here some moduli of elasticity of typical materials, namely nylon, rubber, and wood. These are shown in Table G.1.

Material	Nylon	Rubber	Wood
E $(GPascals)$	2.1-2.8	0.0007-0.004	10-14

Table G.1: Modulus of elasticity E of typical materials [71]

Qualitatively, one can see that a wheat plant is easier to bend than a tree branch of the same diameter. Rubber, on the other hand, is a softer material than a wheat stalk but nylon is harder in bending. As far as the bending properties are concerned, wheat can be described as a hard rubber compound, and for that reason a numerical value of $0.05.10^9$ Pa $(\mathrm{N}.m^{-1})$ is chosen for E_s and E_h. It will be shown later in the section that these values lead to reasonable wheat displacements in the static case.

E_s and E_h are chosen to be identical, because the "method" used to estimate their numerical value is not accurate enough to make any good guess of the difference in bending properties of the stalk and the head.

Wind forcing

The wind forcing is estimated from basic aerodynamics theory. In aerodynamics terms the force to estimate here is the drag exerted on a cylinder in a flow of air of velocity V_∞ far away from the cylinder. The drag D is related to the velocity by [72]:

$$D = \frac{1}{2} C_D \rho_\infty S V_\infty^2 \tag{G.13}$$

where C_D is the drag coefficient, ρ_∞ is the density of air in the steady flow (ρ_∞=1.23 kg.m^{-3} in standard sea level conditions), and S is a reference surface area characteristic of the cylinder (S=2Rl, where R is the radius and l the length of the cylinder).

The drag coefficient for a cylinder is plotted as a function of the Reynolds number R_e in [72], R_e being defined as:

$$R_e = \frac{\rho_\infty V_\infty 2R}{\mu_\infty} \tag{G.14}$$

where μ_∞ is the freestream viscosity coefficient (μ_∞=1.789.$10^{-5} kg.m^{-1}.s^{-1}$ in standard sea level conditions). For values of R of the order of the wheat head and stalk radii, R_e is of the order of 10^3 (dimensionless), which corresponds to a drag coefficient of approximately 1 [72]. The wind force per unit length q_{0s} at the top of the stalk is calculated from:

$$q_{0s} = \frac{D}{L_s} = \frac{C_D q_\infty S}{L_s} = C_D R_s \rho_\infty V_\infty^2 \tag{G.15}$$

And similarly for the force per unit length on the wheat head q_{0h}.

Experimental results on a wheat field presented in [45] have shown that the wind velocity within the canopy varies approximately linearly with height. Since the drag is proportional to the square of the wind velocity, the variation with height of the wind force on the wheat is quadratic. This is the assumption announced in Equation (G.1), which is now justified from aerodynamics fundamentals and experimental results.

Shape function of the wheat

The shape of the wheat stalk under a wind speed of 2 $m.s^{-1}$ at the top of the canopy is plotted in Figure G.3. The deformation occurs mostly at the base of the plant, as observed in the real case. The amplitude of the deflection at 80 cm is about 5.5 cm, which is of the order of magnitude of the displacements measured in the wheat field. This good quantitative agreement between the model deflections and the measured deflections gives confidence in the parameters estimated, especially for the values of E_s and E_h.

G.3 Conclusion on the wheat model

The general theory of structural statics was used here to model the motion of wheat under the influence of wind. The approach developed here is conventionally applied to civil engineering problems, and its application to a crop is novel, although it does not required additional theoretical development. The numerical application to the wheat case is developed as follows:

- all geometrical parameters (length, radius, area moment of inertia) and masses are estimated by direct measurements on the wheat,

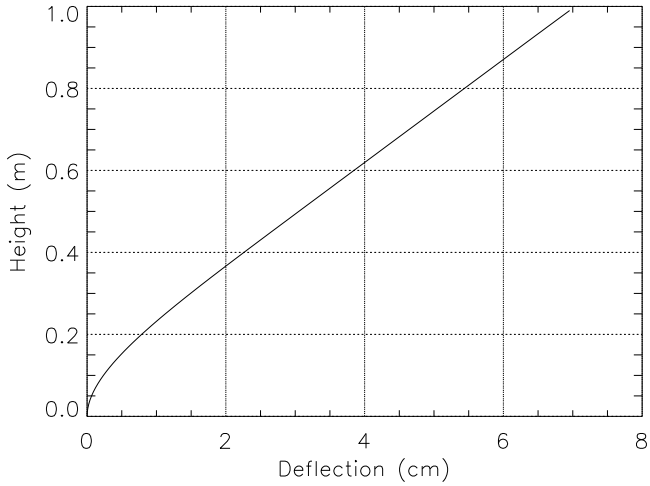

Figure G.3: Modelled shape of the wheat stalk under a wind speed of 2 $m.s^{-1}$ at a height above ground of 0.7 m, and using the numerical values detailed in section G.2

- the modulus of elasticity E is estimated from existing tables of other materials similar to the wheat material (rubber, wood), and to match the deflections of the wheat measured *in situ*,
- the wind force is estimated from basic aerodynamics theory, where the drag force can be related to the wind velocity. The distribution of this force along the wheat plant is estimated from wind measurements within the wheat canopy presented in an independent study.

With this approach, the *in situ* measurements of wind velocity and wheat motion made during this research can be viewed as valuable calibration data. However, one limitation of the model is to be noted here. The model considered a single wheat plant, and the effect of leaves was not accounted for. It is probable that direct contact between adjacent plants and the presence of leaves around the wheat stalk increase the total load on the wheat plant of interest. It is difficult to quantify this effect in the approach presented here. If necessary, the effect of contact between plants and of additional load from the leaves can be represented as an additional force acting on the stalk and the head. For reasons linked to the difficulties associated with quantifying this force, it was not modelled here.

Appendix H

The ERS Tandem data

H.1 Available Tandem pairs

Table H.1 presents the ERS data processed for the research. For each date, the table specifies the satellite which recorded the data (E1 and E2 refer to ERS-1 and ERS-2 respectively), the orbit number, the track/frame combination, the time of the pass over Cranfield, the estimated incidence angle θ at Cranfield (calculated from the position of Cranfield in the full scene) and the perpendicular baseline B_n between the two satellites. The perpendicular baselines are available on the ESA's 'EarthNet Online' Web server (http://earthnet.esrin.esa.it/).

	Date (yymmdd)	Day n°	Sat.	Orbit	Track	Frame	Time	Pass (A/D)	θ (°)	B_n (m)
1	19950606	157	E1	20351	323	2547	10:57	D	23.8	124
	19960607	158	E2	678	323	2547	10:58	D		
2	19950625	176	E1	20623	94	2547	11:00	D	21	98
	19950626	177	E2	950	94	2547	11:00	D		
3	19950711	192	E1	20852	323	2547	10:57	D	23.8	-36
	19950712	193	E2	1179	323	2547	10:58	D		
4	19950730	211	E1	21124	94	2547	11:00	D	21	15
	19950731	212	E2	1451	94	2547	11:00	D		
5	19950815	227	E1	21353	323	2547	10:57	D	23.8	49
	19950816	228	E2	1680	323	2547	10:58	D		
6	19950903	246	E1	21625	94	2547	11:00	D	21	76
	19950904	247	E2	1952	94	2547	11:00	D		
7	19951008	281	E1	22126	94	2547	11:00	D	21	-398
	19951009	282	E2	2453	94	2547	11:00	D		
8	19960102	2	E1	23357	323	2547	10:57	D	23.8	144
	19960103	3	E2	3684	323	2547	10:57	D		
	19960216	47	E1	24008	473	1035	22:06	A		-173
	19960217	48	E2	4335	473	1035	22:06	A		
9	19960225	56	E1	24130	94	2547	11:00	D	21	-35
	19960226	57	E2	4457	94	2547	11:00	D		
10	19960312	72	E1	24359	323	2547	10:57	D	23.8	8

(continued next page)

	Date (yymmdd)	Day n°	Sat.	Orbit	Track	Frame	Time	Pass (A/D)	θ (°)	B_n (m)
	19960313	73	E2	4686	323	2547	10:58	D		
11	19960331	91	E1	24631	94	2547	11:00	D	21	89
	19960401	92	E2	4958	94	2547	11:00	D		
	19960407	98	E1	24738	201	1035	22:03	A		-76
	19960408	99	E2	5065	201	1035	22:03	A		
12	19960416	107	E1	24860	323	2547	10:57	D	23.8	70
	19960417	108	E2	5187	323	2547	10:58	D		
13	19960505	126	E1	25132	94	2547	11:00	D	21	69
	19960506	127	E2	5459	94	2547	11:00	D		

Table H.1: ERS Tandem data pairs processed for the research

H.2 Extracts from the full size data files

Sub-scenes of 600 columns x 3000 lines were extracted from the data tapes containing the SLC data in quadrants. Each sub-scene covers a surface area of 15x15 km. Table H.2 gives the date of the image, the quadrant total size, the origin of the 15x15km extract in the full quadrant, the position of Cranfield in the extract and in the quadrant. The positions are given with an estimated error of 3 pixels in range and 15 pixels in azimuth. The coordinates given for Cranfield are those of the pixel located at the intersection of the two main runways of the Cranfield airfield.

The origin of the pixel coordinates in the full scene is at the North-East corner for descending passes and at the South-West corner for ascending passes. The positions of the 15x15 km extract origin and of Cranfield in the full scene are given from this origin. The position of Cranfield in the 15x15 km extracts is always given from the top left corner of the image.

	Image date (yyyymmdd)	Full scene size		Extract origin in full scene		Cranfield in sub-scene		Cranfield in full scene	
		cols.	lines	cols.	lines	cols.	lines	cols.	lines
1	19950606	26320	4900	2557	23295	299	1980	2858	25275
	19950607	26387	4900	2634	23380	296	1890	2938	25270
2	19950625	26317	4900	396	20780	300	1500	696	22280
	19950626	26247	4900	365	20984	300	1500	665	22484
3	19950711	26316	4900	2602	23300	450	1755	2902	25055
	19950712	26282	4900	2703	23250	450	2015	3003	25265
4	19950730	26352	4900	469	20766	291	1500	778	22266
	19950731	26187	4900	573	20995	292	1500	881	22495
5	19950815	26316	4900	2441	23310	450	1765	2741	25075
	19950816	26349	4900	2675	23340	450	1910	2975	25250
6	19950903	26351	4900	539	20589	304	1500	835	22089
	19950904	26316	4900	531	20696	300	1485	831	22181

(continued next page)

	Image date (yyyymmdd)	Full scene size		Extract origin in full scene		Cranfield in sub-scene		Cranfield in full scene	
		cols.	lines	cols.	lines	cols.	lines	cols.	lines
7	19951008	26337	4900	497	20530	291	1500	788	22030
	19951009	27416	4900	478	20672	299	1500	777	22172
8	19960102	26193	4900	2971	23190	300	1970	3271	25160
	19960103	26651	4900	2669	23650	300	2185	2969	25835
	19960216	26253	4900	2584	17620	301	1500	2885	19120
	19960217	26162	4900	2870	17431	299	1500	3169	18931
9	19960225	26290	4900	490	20859	292	1515	782	22374
	19960226	26339	4900	479	21047	300	1500	779	22547
10	19960312	26212	4900	2651	22805	300	1500	2951	24305
	19960313	26334	4900	2648	22990	300	1500	2948	24490
11	19960331	26335	4900	523	20414	301	1495	824	2190
	19960401	26286	4900	529	21099	300	1500	829	22599
12	19960416	26384	4900	2852	23380	300	1912	3152	25292
	19960417	26352	4900	2837	23350	302	2670	3135	26020
13	19960505	26187	4900	477	20370	300	1500	777	21870
	19960506	26211	4900	481	20980	299	1505	780	22485

Table H.2: Position of the 15x15 km extracts from the data tapes and location of Cranfield in the extracts and in the full scenes

Appendix I

Inputs to the ISAR interferogram generator

In order to generate the output files, ISAR executes a series of subroutines which are compiled in a main program (called Main.x). Some of the subroutines can be executed several times if the user specifies so in a parameter file . The required format for the input files is binary, 32 bit floating point. The SLC data on tape being stored as 16 bit integer values, a format conversion is needed before running ISAR. The data are interleaved by pixel, i.e. the real and imaginary parts of each pixel are stored one after the other, pixel by pixel.

The parameter file contains all input parameters required by ISAR for the computation. It contains file specifications, orbital parameters, filter parameters, window dimensions, and other computational parameters. In total 64 parameters are needed by ISAR.

File specifications

The paths and filenames for the input and output files need to be specified. The sizes of the input files in range and azimuth are also required.

Orbital parameters

ISAR can run with or without the specification of the orbital parameters for the satellites. The orbital parameters to be entered include the satellite altitudes, the latitude of closest approach, and some information concerning the processing of the data (system carrier frequency, Nyquist frequency, ...). The information is given on the tape containing the corresponding SLC data, in the leader file. The ISAR manual gives the line numbers of the leader file where the relevant parameters can be found. ISAR can also run without orbital parameters. The main difference between the two options lies in the estimation of the surface topography. It is an important step in the coherence image generation process because ISAR uses the slope information to filter away the non-overlapping parts of the spectrum of each pixel between the two SAR images. This is the common band filtering operation described in section 2.2.5. For better accuracy, the use of the orbital parameters is recommended but small errors in the value of these parameters (e.g. satellite

altitude) can lead to bigger errors in the output files.

The coherence images for the available tandem pairs were generated with a 3x15 pixel window (range x azimuth). ISAR was run without the orbital parameters because it appeared that some of them were missing from the leader file. The two missing parameters are the 'image sampling window start time' and the 'image absolute first sample'. It is not clear from the ISAR manual how these parameters can be retrieved or at least approximated, so it was decided not to use the orbital parameters in order to avoid introducing more errors in the output results.

Filter parameters

Some filters are used by ISAR to reduce the noisy aspect of the interferogram. They require the definition of cut-off frequencies or bandwidths. In the research the default values have been used for all ISAR runs.

Window dimensions

ISAR uses a certain number of windows in the processing. The sizes are given in pixels in the range and azimuth directions. The windows to be defined are:

- The cross-correlation windows, used for fine registration of the two SLC images. One of the ISAR subroutines finds the shift and stretch to apply to one image with respect to the other by cross-correlating the amplitudes of the two images in two user-defined windows. These windows are defined by their size and position in the full image.
- The slope estimation windows.
- The coherence estimation windows: as explained in Chapter 2-2-2, the coherence is calculated from a number of pixels in a sub-window. The size of this window needs to be specified in the parameter file.

Computational parameters

These parameters specify the number of loops to be performed by ISAR for the registration of the two input images and for the estimation of the local slopes.

More details on each input of the parameter file and on each subroutine of ISAR is available from [46].